J Fluoresc (2011) 21:901–909
DOI 10.1007/s10895-010-0605-5

ORIGINAL PAPER

Photoactive Ru Complex Embedded in Mesostructured MCM-41 Nanoparticles

Emanuela Bottinelli · Ivana Miletto · Giuseppe Caputo · Salvatore Coluccia · Enrica Gianotti

Received: 30 October 2009 / Accepted: 29 January 2010 / Published online: 23 February 2010

Abstract The synthesis and characterization of photoactive hybrid materials based on $[Ru(bpy)_3]^{2+}$ physically adsorbed within the channels of mesoporous MCM-41 silica nanoparticles is presented. A set of photoactive mesostructured hybrids with different guest loading has been prepared and characterized by X-ray diffraction, High Resolution Transmission Electron Microscopy, volumetric analyses, Diffuse Reflectance UV-Vis and Photoluminescence spectroscopies and lifetime measurements. The hybrids synthesis and the washing procedures, performed to investigate the host-guest interaction and the stability of the complex within the mesopores, didn't affect the integrity of the structure and morphology of MCM-41 nanoparticles. The dispersion of $[Ru(bpy)_3]^{2+}$ within the channels varied depending on the loading value and this is reflected in the different and peculiar photoluminescence features of the resulting hybrid materials. Photoluminescence spectroscopy evidenced that the use of MCM-41 nanoparticles ensures a better dispersion of the complex within the mesopores, if compared with traditional MCM-41. Further studies are in progress to investigate the interesting and promising features exhibited by such photoactive systems for advanced applications of electrochemiluminescence in optoelectronics and diagnostics.

E. Bottinelli · I. Miletto · G. Caputo · S. Coluccia · E. Gianotti
Dipartimento di Chimica IFM and NIS, Centre of Excellence,
University of Turin,
via P. Giuria 7,
10125 Torino, Italy

E. Bottinelli (✉)
NIS Laboratories at Centro dell'Innovazione,
via G. Quarello 11/A,
10135 Torino, Italy
e-mail: emanuela.bottinelli@unito.it

Keywords MCM-41 nanoparticles · $[Ru(bpy)_3]^{2+}$ · Photoactive nanoparticles · Hybrid materials · Photoluminescence

Introduction

The encapsulation of different photoluminescent guest molecules into variously modified mesoporous hosts has been widely investigated in order to obtain new improved photoactive materials and to study how the features of the host (composition, size, morphology, etc.) can affect the photoemission properties of the guest molecules. Several kinds of fluorescent molecules, such as coumarins [1–3], fluoresceins [4, 5], rhodamines [6–8], cyanines [9–11], porphyrins [12], transition metal complexes [13–15], confined within mesoporous siliceous materials such as MCM-41, MCM-48 and SBA-15, have been investigated. Among transition metal complexes, Tris(2,2′-bipyridyl) ruthenium(II), $[Ru(bpy)_3]^{2+}$, is one of the most studied due to its large variety of interesting features, including its strong luminescence, electrochemiluminescence (ECL) high efficiency and relatively high thermal and chemical stability, its solubility in a variety of aqueous and non aqueous solvents at room temperature and its ability to undergo reversible one-electron transfer reactions at easily attainable potentials [16–18]. In the last decade, different hybrids have been studied, in which $[Ru(bpy)_3]^{2+}$ is confined within the core of non porous silica nanoparticles [19, 20] or physically adsorbed within the channels of mesoporous silicas belonging to M41S family [13, 21–24]; in fact, the high specific surface area and the controllable pore size distribution make these mesoporous systems ideal candidates as host materials to guest organic molecules. The effect of the surface functionalisation and of the

hydration of the material on the photophysical properties and on the distribution of the $[Ru(bpy)_3]^{2+}$ molecules have been studied [22]. However, at the best of our knowledge, the effect of the morphology of the host on the dispersion and photoluminescence of $[Ru(bpy)_3]^{2+}$ confined in a mesostructured system has not been well-documented.

In the last period, different synthetic methodologies have been proposed for the preparation of mesoporous silica nanoparticles (NPs) [25–27], that lead to NPs with controlled morphologies and peculiar properties. The shape and the size of the mesostructured NPs allow exploring their potential use as a support in new and specific applications such as drug delivery, optical imaging and also permit the development of smart materials for advanced technologies.

MCM-41-type mesoporous silica NPs with defined dimensions and uniform size distribution offer a suitable nanometer-sized environment for the inclusion of the $[Ru(bpy)_3]^{2+}$ ions characterised by a diameter of 12 Å (Fig. 1b). MCM-41 NPs with homogeneous size distribution and loaded with $[Ru(bpy)_3]^{2+}$ can be of huge interest for the production of films or active surfaces to be used as ECL sensors or optoelectronic devices.

In the present paper, we present the synthesis and the characterization of photoactive hybrid material based on $[Ru(bpy)_3]^{2+}$ physically adsorbed within the channels of MCM-41-type mesoporous silica NPs that are interesting and promising materials for ECL applications. Three hybrid materials at different loading were prepared by increasing $[Ru(bpy)_3]^{2+}$ concentration in the solution. The confinement, the dispersion and the modifications of the optical properties of $[Ru(bpy)_3]^{2+}$ within the mesoporous channels have been investigated by X-ray diffraction (XRD), volumetric analyses, High Resolution Transmission Electron Microscopy (HRTEM), Diffuse Reflectance (DR) UV-Vis and Photoluminescence spectroscopies and lifetime measurements. In order to assess the effect of the morphology of the mesoporous host (MCM-41 homogeneous NPs or bulk MCM-41 composed of inhomogeneous particles in the micrometer range) on the overall dispersion of the $[Ru(bpy)_3]^{2+}$ inside the channels and on the performances of the hybrids, the optical properties of the different hybrid materials were compared to those of the hybrids described in a previous work [21] in which $[Ru(bpy)_3]^{2+}$ was physically adsorbed within the channels of traditional MCM-41.

Experimental

Materials

Tris(2,2′-bipyridyl)ruthenium(II) chloride hexahydrate (hereafter $[Ru(bpy)_3]^{2+}$) was purchased by Sigma-Aldrich and used as received. The structure (Fig. 1a) and the 3D arrangement (Fig. 1b) of the complex are shown in Fig. 1. All other reagents and solvents were purchased by Sigma-Aldrich and used as received.

Methods

Preparation of host MCM-41 nanoparticles

Mesoporous MCM-41 silica NPs were prepared according to literature procedures using cetyltrimethylammonium bromide (CTAB) as structure directing agent (SDA) [27]. CTAB (1 g, 2.74 mmol) was dissolved in 480 ml of distilled water with NaOH (2.0 M, 3.5 ml). When the temperature was adjusted at 80 °C, Tetraethyl Orthosilicate (TEOS) (5 ml, 22.4 mmol) was added dropwise under vigorous stirring. The reaction mixture was then stirred at 80 °C for 2 h. The formed white precipitate was filtered off and washed with water and methanol. The CTAB template was removed from the as-synthesized material by calcination (at 550 °C, for 4 h and 30′ under N_2 flow and subsequently for 7 h under O_2) rather than acidic extraction, in order to completely remove the

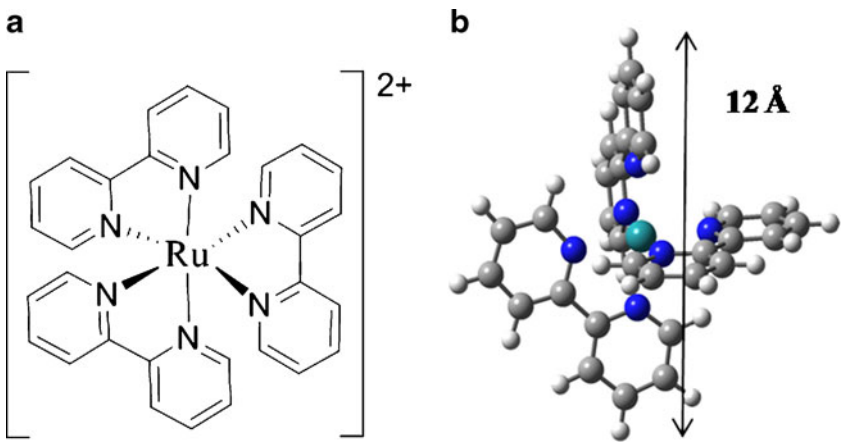

Fig. 1 Section a: structure of the $[Ru(bpy)_3]^{2+}$. Section b: 3D arrangement of the $[Ru(bpy)_3]^{2+}$

SDA and to improve the crystallisation of the silica to obtain a well ordered mesoporous MCM-41 structure.

Synthesis of $[Ru(bpy)_3]^{2+}$/MCM-41 NPs hybrids

MCM-41 NPs were outgassed at 300 °C overnight to remove adsorbed water and then a solutions of $[Ru(bpy)_3]^{2+}$ in acetonitrile was physically adsorbed. The mixture was stirred at room temperature for 2 h, then the solid hybrid was filtered off and dried under vacuum at room temperature. Three hybrid materials were prepared by increasing the $[Ru(bpy)_3]^{2+}$ loading, namely $[Ru(bpy)_3]^{2+}$/MCM-41 NPs 1 mg/g, $[Ru(bpy)_3]^{2+}$/MCM-41 NPs 10 mg/g and $[Ru(bpy)_3]^{2+}$/MCM-41 NPs 100 mg/g. The actual loading of the as-prepared hybrids was evaluated by UV-Vis absorption analysis of the filtered solutions.

Leaching tests Each sample was then washed several times with acetonitrile, until no free ruthenium complex was found in the supernatant. Actual loading after washing procedures was then evaluated by UV-Vis absorption. Nominal and actual loading values before and after washing procedure are summarized in Table 1.

The colour of the different hybrids prepared goes from pale to deep yellow depending on the $[Ru(bpy)_3]^{2+}$ loading.

Physico-chemical characterization

High resolution transmission electron microscopy (HRTEM)

HRTEM observations were performed on a JEOL 3010 instrument operating at 300 kV. For the measurements, NPs powders were dispersed on a copper grid coated with a perforated carbon film. The size distributions of the samples were obtained by measuring ca. 300 particles, and the mean particle diameter (d_m) was calculated as $d_m=\Sigma d_1 n_1/\Sigma n_i$, where n_1 was the number of particles of diameter d_i. The results are indicated as ($d_m \pm$STDV).

X-ray diffraction (XRD)

XRD patterns of pure MCM-41 and hybrid NPs were obtained by a Philips 1830 instrument, operating with Co Kα radiation, generated at 20 mA and 40 kV.

Volumetric analyses

Specific surface area (SSA), cumulative pore volume and pore size distribution were measured by N_2 adsorption-desorption isotherms at 77 K using a Micromeritics ASAP2020 instrument. The SSA was calculated by the Brunauer-Emmett-Teller (BET) method, and the average pore size was evaluated from the adsorption branch of the isotherms using the Barrett-Joyner-Helenda (BJH) method.

UV-Vis absorption, diffuse reflectance (DR) UV-Vis and photoluminescence spectroscopy

UV-Vis absorption spectra were recorded on a Cary 300 instrument for samples in solution and on a Cary 5000 instrument equipped with an integrated sphere, coated with $BaSO_4$, for measurement on solid samples in the diffuse reflectance mode. The reflectance spectra were then elaborated by using the Kubelka Munk function. Photoemission and excitation steady-state spectra were acquired with a Horiba Jobin Yvon Fluorolog3 TCSPC spectrofluorimeter equipped with a 450 W Xenon lamp and a Hamamatsu R928 photomultiplier. The spectral response was corrected for the spectral sensitivity of the photomultiplier. Fluorescence lifetimes were measured using a time-correlated single photon counting (TCSPC) technique (Horiba Jobin Yvon) with excitation source NanoLed at 455 nm (Horiba) and impulse repetition rate of 1 MHz at 90° to a TBX-4 detector. The detector was set to 600 nm with a 5 nm band pass. The instrument was set in the Forward TAC mode, where the excitation pulse represented the start signal by the time-to-amplitude converter (TAC), and the first detected photon triggered the stop signal. DAS6 decay analysis software was used for lifetime calculation.

Results and discussion

Synthesis of the hybrid NPs

Samples with three different $[Ru(bpy)_3]^{2+}$ loadings were prepared: 1 mg/g, 10 mg/g and 100 mg/g. These three loadings were chosen on the basis of a previous work in which $[Ru(bpy)_3]^{2+}$ has been physically adsorbed within

Table 1 Nominal and actual loading values of the hybrid materials before and after acetonitrile washing procedure

Name of Samples	Nominal $[Ru(bpy)_3]^{2+}$ loading (mg/g)	Actual $[Ru(bpy)_3]^{2+}$ loading before washing procedure (mg/g)	Actual $[Ru(bpy)_3]^{2+}$ loading after washing procedure (mg/g)
$[Ru(bpy)_3]^{2+}$/MCM-41NPs 1 mg/g	1	0.99	0.94
$[Ru(bpy)_3]^{2+}$/MCM-41NPs 10 mg/g	10	9.30	8.46
$[Ru(bpy)_3]^{2+}$/MCM-41NPs 100 mg/g	100	86.93	40.86

the channels of MCM-41 [21]. As it can be seen in Table 1, for all the hybrids the actual loading after impregnation was very close to the nominal one. To investigate the interaction between the ruthenium complex and the silica matrix and the stability of $[Ru(bpy)_3]^{2+}$ adsorption inside the mesoporous channels, a leaching test was performed on all the samples, in order to remove the fraction of the complex not strongly interacting with the silica host. Repeated washings of the hybrids with acetonitrile resulted in a heavy leaching of the ruthenium complex from the mesopores in the case of 100 mg/g hybrid and in a moderate leaching for the 10 mg/g. On the contrary, no significant leaching by 1 mg/g hybrid was observed.

Structural and morphological characterization

All the photoactive $[Ru(bpy)_3]^{2+}$/MCM-41 NPs hybrids were characterized by XRD, volumetric analyses and HRTEM in order to obtain information about the effect of the impregnation and washing procedures on the ordered structure, size and morphology of the MCM-41 NPs.

XRD analysis allows investigating the structure of MCM-41 mesoporous silica NPs and monitoring the structural modification of the hybrids before and after the washing procedures. Figure 2 shows XRD patterns of calcined MCM-41-NPs (curve a) and washed hybrids [Ru $(bpy)_3]^{2+}$/MCM-41 NPs 1 mg/g (curve b), $[Ru(bpy)_3]^{2+}$/MCM-41 NPs 10 mg/g (curve c) and $[Ru(bpy)_3]^{2+}$/MCM-41 NPs 100 mg/g (curve d).

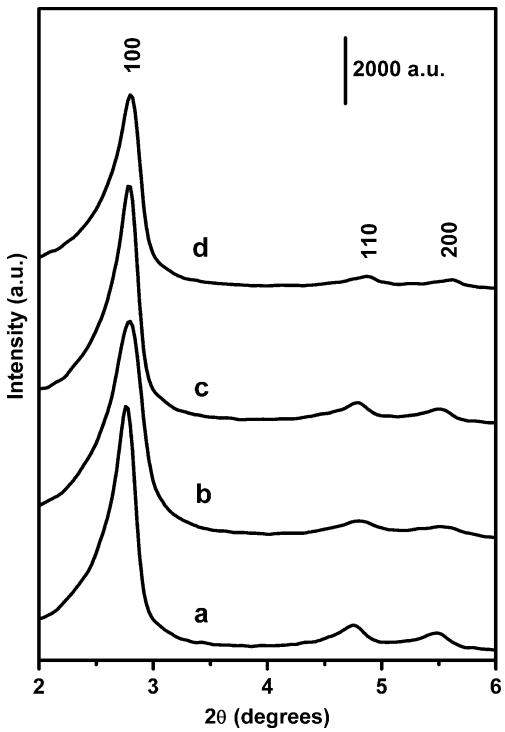

Fig. 2 XRD diffraction patterns of calcined MCM-41 NPs (*curve a*), $[Ru(bpy)_3]^{2+}$/MCM-41 NPs 1 mg/g washed (*curve b*), $[Ru(bpy)_3]^{2+}$/MCM-41 NPs 10 mg/g washed (*curve c*) and $[Ru(bpy)_3]^{2+}$/MCM-41 NPs 100 mg/g washed (*curve d*)

XRD pattern of calcined MCM-41 NPs showed the (100), (110), and (200) reflections that are typical of an ordered mesostructured silica which exhibits a regular pore system consisting of a hexagonal array of unidimensional channels [28]. All the hybrids are characterized by the same pattern, indicating that neither the impregnation, nor the washing procedures affected the structural integrity of MCM-41 NPs. A decrease in the diffraction intensity for the three main peaks in the hybrid with the highest loading ($[Ru(bpy)_3]^{2+}$/MCM-41 NPs 100 mg/g) could indicate a slight reduction of the degree of order for the hexagonal arrangement occurred during the impregnation [29, 30].

The HRTEM image of calcined MCM-41 NPs (Fig. 3a) showed the presence of nanostructured MCM-41 NPs, with an average particle size of (100± 23) nm, characterized by regular and ordered channels with hexagonal symmetry. In all cases, HRTEM analysis evidenced that both the ordered mesoporous structure and the nanoparticles morphology were retained after the impregnation and the washing procedures. As an example, HRTEM images of $[Ru(bpy)_3]^{2+}$/MCM-41 NPs 1 mg/g before (Fig. 3b) and after (Fig. 3c) the washing procedure are reported.

In order to evaluate the porosity and volumetric characteristics of MCM-41 NPs and to elucidate the dispersion of $[Ru(bpy)_3]^{2+}$ into the channels of mesostructured NPs, calcined MCM-41 NPs and $[Ru(bpy)_3]^{2+}$/MCM-41 NPs hybrids were characterized by volumetric analyses. The "type IV" N_2 adsorption-desorption isotherms with H1-type hysteresis, typical of mesoporous materials with one-dimensional cylindrical channels, can be observed for all the prepared samples. In particular, the sharp inflection at 0.25–0.35 p/p° corresponding to the capillary condensation within the mesopores and the hysteresis loop at pressure above 0.9 p/p°, due to condensation in textural porosity, are present in all the samples. The BET surface area, average pores diameter and pores volume of calcined MCM-41-NPs and washed hybrids are reported in Table 2.

In comparison with the calcined MCM-41 NPs (SSA of ca.1050 m^2/g and average pore diameter ca. 21 Å) only a slight decrease in the SSA and in the mean pores diameter is observed in the case of 1 mg/g and 10 mg/g samples, whereas for the hybrid with the highest loading (100 mg/g), these parameters are more reduced with respect to the plain MCM-41 NPs. The decrease in the SSA, pore volume and pore diameter confirms that most of the Ru complexes is confined inside the mesopores of MCM-41 NPs.

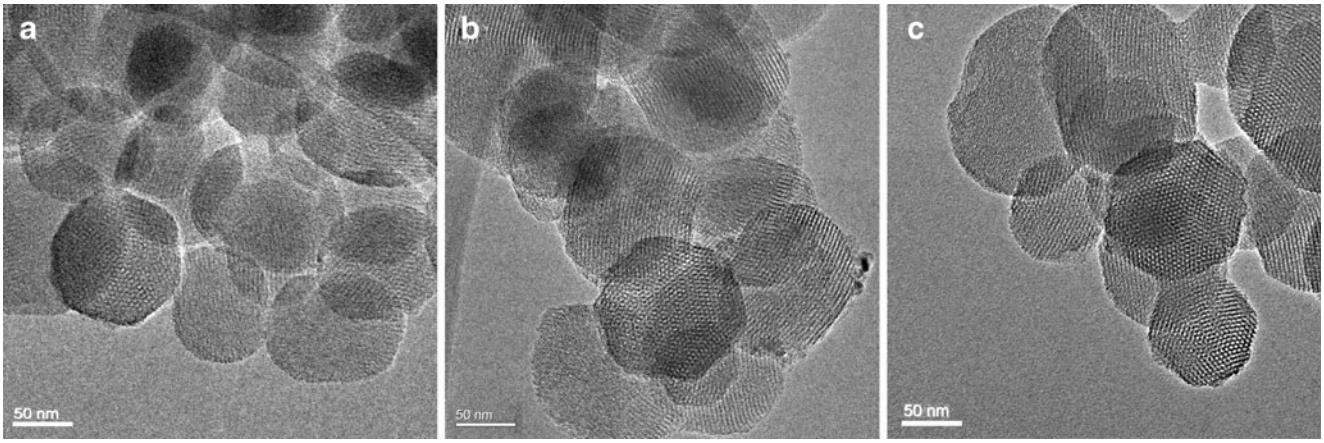

Fig. 3 HRTEM images of calcined MCM-41 NPs and of $[Ru(bpy)_3]^{2+}$ hybrids. Section a: calcined MCM-41 NPs. Section b: $[Ru(bpy)_3]^{2+}$/MCM-41 NPs 1 mg/g before washing procedure. Section c: $[Ru(bpy)_3]^{2+}$/MCM-41 NPs 1 mg/g after washing procedure

UV-Vis absorption and photoemission of hybrids

DR-UV-Vis spectra of the as-synthesised hybrids and of the hybrids obtained after washing procedure are reported in Fig. 4 (section A), along with the spectrum of the complex in acetonitrile solution (section B) for the sake of comparison. Typical absorption spectrum of $[Ru(bpy)_3]^{2+}$ is characterised by an intense band in the visible region, centred at 450 nm with a bathochromic shoulder at 420 nm, that is assigned to metal-to-ligand charge transfer (MLCT) transitions in which an electron is promoted from the Ru t_{2g} orbital to the π^* orbital of the bipyridine ligands.

The weak components at ca. 350 nm and 323 nm are attributable to metal-centred (MC) *d-d* transitions, as well as the partially resolved twin peaks at 238 and 250 nm. The intense band at 285 nm, as well as the absorptions at 185 nm and 208 nm, are easily assigned to ligand centred (LC) π-π^* transitions, by comparison with the spectrum of the protonated bipyridine (bpy) ligands [18]. As in the case of $[Ru(bpy)_3]^{2+}$/MCM-41 hybrids described in our previous work [21], all the$[Ru(bpy)_3]^{2+}$/MCM-41 NPs samples with increasing loading showed no significant differences in the position of the absorption maxima with respect to $[Ru(bpy)_3]^{2+}$ in acetonitrile solution. The absorbance increases along with the increase in $[Ru(bpy)_3]^{2+}$ concentration, as observed before for $[Ru(bpy)_3]^{2+}$/MCM-41 hybrids; the same trend was also observed after the washing procedures. Moreover, along with the increase in the loading, a strong decrease in the intensity of the LC band at 285 nm occurs. In literature such a behaviour was observed for similar materials and it was assigned to the formation of covalently hydrated or slightly distorted bpy ligands [18, 31]. Further studies are in progress to better elucidate this point.

The photoluminescence spectra of as-synthesised and washed $[Ru(bpy)_3]^{2+}$/MCM-41 NPs hybrids are reported in Fig. 5 (section A); the spectrum of $[Ru(bpy)_3]^{2+}$ in acetonitrile is also reported (section B) for the sake of comparison.

The emission intensity increases along with the increase in $[Ru(bpy)_3]^{2+}$ loading but without direct proportionality; this evidence suggested that probably a slight concentration quenching occurs within the channels of MCM-41 NPs. In the case of washed samples, for the hybrid with the highest loading ($[Ru(bpy)_3]^{2+}$/MCM-41 NPs 100 mg/g) the drop in emission intensity after the washing procedure is smaller with respect to the drop in DR-UV-Vis intensity. Nevertheless, the same emission intensity trend described before is also maintained for the washed samples. As we noticed in our previous work [21], a heavy concentration quenching

Table 2 Specific surface area (SSA), cumulative pore volume and average pore diameter values in calcined MCM-41 NPs, $[Ru(bpy)_3]^{2+}$/MCM-41 1 mg/g after washing procedure, $[Ru(bpy)_3]^{2+}$/MCM-41 10 mg/g after washing procedure and $[Ru(bpy)_3]^{2+}$/MCM-41 100 mg/g after washing procedure

Samples	SSA (m^2/g)	Cumulative pore volume (cm^3/g)	Average pore diameter (Å)
Calcined MCM-41 NPs	1,050	0.97	21
$[Ru(bpy)_3]^{2+}$/MCM-41 NPs 1 mg/g washed	945	0.84	20
$[Ru(bpy)_3]^{2+}$/MCM-41 NPs 10 mg/g washed	914	0.78	20
$[Ru(bpy)_3]^{2+}$/MCM-41 NPs 100 mg/g washed	892	0.55	19

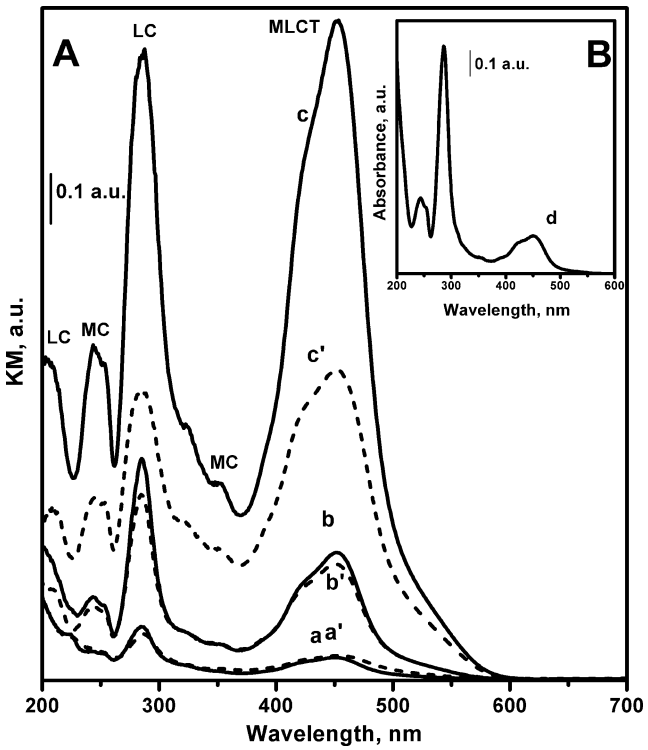

Fig. 4 Comparison between DR-UV-Vis spectra of $[Ru(bpy)_3]^{2+}$ hybrids. Section A: $[Ru(bpy)_3]^{2+}$/MCM-41 NPs 1 mg/g before (a) and after washing procedure (a′); $[Ru(bpy)_3]^{2+}$/MCM-41 NPs 10 mg/g before (b) and after washing procedure (b′); $[Ru(bpy)_3]^{2+}$/MCM-41 NPs 100 mg/g before (c) and after washing procedure (c′). Section B: $[Ru(bpy)_3]^{2+}$ in acetonitrile

effect occurred in $[Ru(bpy)_3]^{2+}$/MCM-41 hybrid materials, thanks to which the emission intensity increased along with the decrease in $[Ru(bpy)_3]^{2+}$ concentration within the channels of MCM-41. We can therefore conclude that the use of MCM-41 NPs instead of bulk MCM-41 as host for $[Ru(bpy)_3]^{2+}$ molecules leads to a better dispersion of the complex within the channels of the mesoporous silica material. It has also to be noticed that the emission spectra of unwashed sample undergo a progressive red shift along with the increase of the loading, suggesting that different states of the adsorbed $[Ru(bpy)_3]^{2+}$ are present at different loadings. The red shift is assignable to the fact that the excited state of $[Ru(bpy)_3]^{2+}$ has an asymmetric single-ligand-localised (bpy)* $[Ru(bpy)_2]^{2+}$ charge distribution with a higher energy and when $[Ru(bpy)_3]^{2+}$ is entrapped in MCM-41 NPs at low loading, it is supposed that all the molecules are isolated and the excited (bpy)* ligand has no correlation with other bpy ligands. As a consequence, the excited state is not stabilized and the emission is produced at higher energy. When the loading increases, the excited (bpy)* ligand can interact with the ligands of adjacent molecules and the electrons of (bpy)* can be delocalized onto the adjacent bpy ligands, determining a decrease in the excited state energy [21]. The wavelength trend is the same for washed sample, with the exception of the 1 mg/g sample, whose emission spectrum is 10 nm red shifted with respect to the correspondent unwashed sample. The emission wavelength of the highest loading hybrid is that of $[Ru(bpy)_3]^{2+}$ in acetonitrile solution (610 nm), whilst 10 mg/g and 1 mg/g samples are characterised by an emission band centred at 600 nm and 590 nm respectively. The observed wavelength blue shift with respect to the complex in solution is in accordance with what observed by Ogawa et al. [22]; they ascribe this effect to the interactions between $[Ru(bpy)_3]^{2+}$ and silica surface. The washing procedures lead to a decrease of the photoemission intensity, coherent with the leaching values listed in Table 1 and already discussed.

In order to better elucidate $[Ru(bpy)_3]^{2+}$ distribution (location of the complex on the surface or within the channels) and dispersion (arrangement, e.g. uniform dispersion or aggregation) within the channels of MCM-41 NPs, fluorescence lifetimes were measured and the data compared with lifetime values of $[Ru(bpy)_3]^{2+}$ in acetonitrile solution and of $[Ru(bpy)_3]^{2+}$ in MCM-41 at different loading (Table 3).

The decay of $[Ru(bpy)_3]^{2+}$ in solution followed mono-exponential kinetics, whilst the decay traces of the hybrid materials were fitted by a bi-exponential decay function. Hybrid materials has two different lifetimes values, corresponding to two different silica microenvironments around $[Ru(bpy)_3]^{2+}$ complexes. The longer lifetime (here-

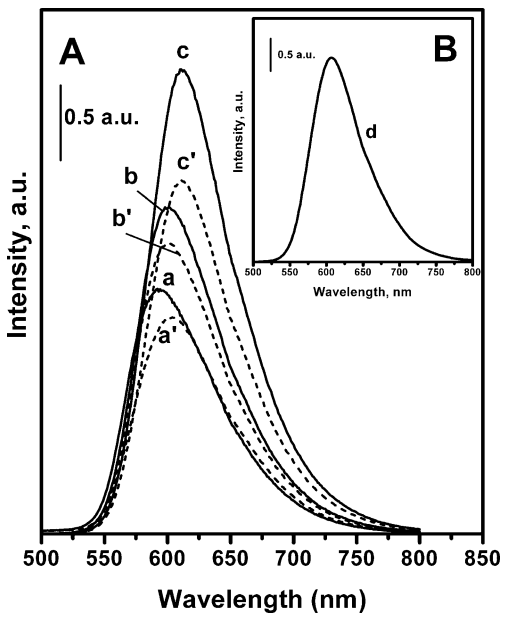

Fig. 5 Comparison between fluorescence spectra (λ_{exc}=450 nm) of [Ru $(bpy)_3]^{2+}$ hybrids. Section A: $[Ru(bpy)_3]^{2+}$/MCM-41 NPs 1 mg/g before (a) and after washing procedure (a′); $[Ru(bpy)_3]^{2+}$/MCM-41 NPs 10 mg/g before (b) and after washing procedure (b′); $[Ru(bpy)_3]^{2+}$/MCM-41 NPs 100 mg/g before (c) and after washing procedure (c′). Section B: [Ru $(bpy)_3]^{2+}$ in acetonitrile

Table 3 Lifetime data of $[Ru(bpy)_3]^{2+}$ in acetonitrile and of hybrid materials

Samples		Lifetimes values[a]		χ^2
		τ_1/ns	τ_2/ns	
$Ru(bpy)_3^{2+}$ solution[b]		135.5±0.4 (100%)	–	1.05
$Ru(bpy)_3^{2+}$ 1 mg/g	MCM-41[c]	140±15 (21%)	799±24 (79%)	0.99
	MCM-41 NPs	120±4 (21%)	1,034±13 (72%)	1.08
	MCM-41 NPs washed	241±11 (32%)	793±8 (68%)	1.00
$Ru(bpy)_3^{2+}$ 10 mg/g	MCM-41[c]	69±3 (41.5%)	588±20 (58.5%)	0.97
	MCM-41 NPs	165±6 (29%)	769±6 (71%)	1.05
	MCM-41 NPs washed	136±5 (28%)	823±7 (72%)	1.25
$Ru(bpy)_3^{2+}$ 100 mg/g	MCM-41[c]	60±6 (25.6%)	433±20 (74.4%)	1.00
	MCM-41 NPs	259±12 (29%)	644±5 (71%)	1.19
	MCM-41 NPs washed	195±11 (20%)	618±3 (80%)	1.19

[a] Lifetime values are expressed as ns ± ST.DV (Relative Amplitude)

[b] in acetonitrile 1 μM

[c] [21]

after τ_2) could be assigned to guest molecules surrounded by silanols inside the pores, that are much more constrained and account for ca. 70% of the species, whilst the shorter lifetime (hereafter τ_1) could be due to $[Ru(bpy)_3]^{2+}$ complexes surrounded by silanols present on the external silica surface (ca. 30%) [11].

Two different approaches can be used to interpret the lifetime data: i) considering the effect of the host morphology, thus by comparing $[Ru(bpy)_3]^{2+}$/MCM-41 and $[Ru(bpy)_3]^{2+}$/MCM-41 NPs samples, and ii) considering the effect of the washing procedure on the $[Ru(bpy)_3]^{2+}$/MCM-41 NPs hybrids.

The hypothesis of a better dispersion of $[Ru(bpy)_3]^{2+}$ within the channels of MCM-41 NPs with respect to MCM-41, already done on the basis of the absence of heavy concentration quenching in the case of MCM-41 NPs hybrids, found a confirmation from the comparison of the lifetime values.

Focusing on τ_2 and comparing $[Ru(bpy)_3]^{2+}$/MCM-41 to unwashed $[Ru(bpy)_3]^{2+}$/MCM-41 NPs hybrids, we can notice that it decreases along with the increase in the loading, in the case of both MCM-41 and MCM-41 NPs; despite the same trend, it has to be noticed that the lifetimes values are longer in the case of MCM-41 NPs samples, suggesting that the use of NPs ensures a better dispersion of $[Ru(bpy)_3]^{2+}$ within the channels of the mesoporous host. This better dispersion reduces deactivations of excited states of $[Ru(bpy)_3]^{2+}$ complexes by interaction with each others, extending the fluorescence lifetime. The trend is different in the case of τ_1: its value decreases along with the increase in complex loading for the MCM-41 hybrids series, on the contrary, in MCM-41 NPs hybrids the value of the shorter lifetime increases along with the increase in $[Ru(bpy)_3]^{2+}$ content. The different behaviour could be due to the fact that for the same volume, MCM-41 NPs have a higher external surface than bulk MCM-41, therefore $[Ru(bpy)_3]^{2+}$ molecules located on the external surface do not undergo radiationless deactivation through interactions with each other.

The effect of the washing procedure on $[Ru(bpy)_3]^{2+}$/MCM-41 NPs samples is of difficult interpretation and although in all the cases there is no significant variation of the relative amplitude of the two populations, a general trend is not observable. In the case of the lower loading, despite no significant leaching was observed, a significant shortening of τ_2 occurs, along with an increase in τ_1. Conversely, 10 mg/g $[Ru(bpy)_3]^{2+}$/MCM-41 NPs hybrid exhibited a decrease of τ_1 and an increase of τ_2 along with the washing procedure. In the case of the higher loading sample, both the lifetime values decreases after the washing. This heterogeneous behaviour suggests that something more than simple leaching occurs inside the channels and on the external surface. As suggested by Ogawa et al. [22] the interaction between $[Ru(bpy)_3]^{2+}$ and the silica surface is weak; therefore, the state of the adsorbed $[Ru(bpy)_3]^{2+}$ can be varied by co-adsorbing species. We can hypothesize that the washing procedure causes a rearrangement of $[Ru(bpy)_3]^{2+}$ molecules, both within the pores and on the external surface, leading to the observed heterogeneous effects on the fluorescence lifetimes. We believe that this hypothesis could also support the anomalous 10 nm red-shift of the emission spectrum observed for the washed $[Ru(bpy)_3]^{2+}$/MCM-41 1 mg/g hybrid. Further studies to better elucidate this observed behaviour are in progress.

Conclusions

In this study, photoactive hybrid materials with specific photoluminescence properties have been successfully synthesized by physically adsorbing $[Ru(bpy)_3]^{2+}$ complex and tuning its loading into the channels of MCM-41-type mesoporous silica nanoparticles.

As demonstrated by XRD, HRTEM and volumetric analyses, neither the impregnation, nor the washing procedures, useful to investigate the interaction between

the ruthenium complex and the silica matrix, affected the integrity of the mesoporous structure and of the nanoparticles morphology.

The nanostructured spaces of mesoporous MCM-41 NPs afford effective two-dimensional environments for orientation and immobilization of the ruthenium complex. The distribution and dispersion of $[Ru(bpy)_3]^{2+}$ within the channels varied depending upon the $[Ru(bpy)_3]^{2+}$ loading value and this is reflected in the different and peculiar photoluminescence features of the resulting hybrid materials.

Finally, the assessment of the effect of the morphology of the mesoporous host on the overall dispersion of the $[Ru(bpy)_3]^{2+}$ inside the channels evidenced that the use of MCM-41 NPs instead of bulk MCM-41 ensures a better dispersion of the complex within the mesopores.

Preliminary investigations to evaluate the redox and electrochemiluminescence properties of this hybrid systems showed that the $Ru(bpy)_3^{2+}$ embedded in mesostructure MCM-41 nanoparticles maintained its ECL high efficiency (data not shown). Further studies are in progress to investigate these interesting and promising features for advanced applications in optoelectronics and as novel ECL sensor devices with improved efficiency, high sensitivity and reactivity.

Acknowledgments This work has been carried out in the frame of the Regione Piemonte CIPE 2004, D67 project. The authors acknowledge Compagnia di San Paolo for sponsorship to NIS—Centre of Excellence. IM thanks Piedmont Region for financial support. Authors would like to thanks Mr G. Bonagemma. Authors are also grateful to Prof. P. Civera, Prof. D. Demarchi and Dott. R. Canova (CHI-Lab Laboratory—DELEN Dipartimento di Elettronica—Politecnico di Torino) for preliminary ECL investigations.

References

1. Zhao W, Li D, He B, Zang J, Huang J, Zang L (2005) The photoluminescence of coumarin derivative encapsulated in MCM-41 and Ti-MCM-41. Dyes Pigm 64(3):265–270
2. Li D, Zang J, Anpo M, Xue M, Liu Y (2005) Photophysical and photochemical properties of Coumain-6 molecules incorporated within MCM-48. Mater Lett 59(17):2120–2123
3. Gu G, Ong PP, Li Q (1999) Photoluminescence of coumarin 540 dye confined in mesoporous silica. J Phys D: Appl Phys 32 (17):2287–2289
4. Yao Y, Zhang M, Shi J, Gong M, Zhang H, Yang Y (2001) Encapsulation of fluorescein into MCM-41 mesoporous molecular sieve by a sol–gel method. Mater Lett 48(1):44–48
5. Lin YS, Lin YS, Tsai CP, Huang HY, Kuo CT, Hung Y, Huang DM, Chen YC, Mou CY (2005) Well-ordered mesoporous silica nanoparticles as cell markers. Chem Mater 17(18):4570–4573
6. Seçkin T, Gultek A, Kartaca S (2003) The grafting of Rhodamine B onto sol-gel derived mesoporous silicas. Dyes Pigm 56(1):51–57
7. Wang L, Lei J, Zhang J (2009) Building of multifluorescent mesoporous silica nanoparticles. Chem Commun 16:2195–2197
8. He Q, Shi J, Cui X, Zhao J, Chen Y, Zhou J (2009) Rhodamine B-co-condensed spherical SBA-15 nanoparticles: facile co-condensation synthesis and excellent fluorescence features. J Mater Chem 19 (21):3395–3403
9. Xu W, Guo H, Akins DL (2001) Aggregation and exciton emission of a cyanine dye encapsulated within mesoporous MCM-41. J Phys Chem B 105(32):7686–7689
10. Xu W, Akins DL (2002) Absorption and exciton emission by an aggregated cyanine dye occluded within mesoporous SBA-15. J Phys Chem B 106(8):1991–1994
11. Gianotti E, Bertolino CA, Benzi C, Nicotra G, Caputo G, Castino R, Isidoro C, Coluccia S (2009) Photoactive hybrid nanomaterials: indocyanine immobilized in mesoporous MCM-41 for "In-Cell" bioimaging. ACS Appl Mater Interfaces 1(3):678–687
12. Xu W, Guo H, Akins DL (2001) Aggregation of tetrakis(p-sulfonatophenyl)porphyrin within modified mesoporous MCM-41. J Phys Chem B 105(8):1543–1546
13. Ogawa M, Nakamura T, Mori J-I, Kuroda K (2001) Incorporation of tris(2, 2′-bipyridine)ruthenium(II) cations ([Ru(bpy)3]2+) into a mesoporous silica. Microporous Mesoporous Mater 48(1–3):159–164
14. Tiseanu C, Parvulescu VI, Kumke MU, Dobroiu S, Gessner A, Simon S (2009) Effects of support and ligand on the photoluminescence properties of siliceous grafted europium complexes. J Phys Chem C 113(14):5784–5791
15. Lu XB, Zhang WH, He R (2002) Simultaneous removal of surfactant template from MCM-41 and implantation of transition metal complexes into mesopores with supercritical fluid. Chinese Chem Lett 13(5):480–483
16. Richter MM (2004) Electrochemiluminescence (ECL). Chem Rev 104(6):3003–3036
17. Innocenzi P, Kozuka H, Yoko T (1997) Fluorescence properties of the Ru(bpy)(3)(2+) complex incorporated in sol-gel-derived silica coating films. J Phys Chem B 101(13):2285–2291
18. Kalyanasundaram K (1982) Photophysics, photochemistry and solar energy conversion with tris(bipyridyl)ruthenium(II) and its analogues. Coord Chem Rev 46:159–244
19. Santra S, Zhang P, Wang KM, Tapec R, Tan W (2001) Conjugation of biomolecules with luminophore-doped silica nanoparticles for photostable biomarkers. Anal Chem 73 (20):4988–4993
20. Bagwe RP, Yang C, Hilliard LR, Tan W (2004) Optimization of dye-doped silica nanoparticles prepared using a reverse microemulsion method. Langmuir 20(19):8336–8342
21. Bottinelli E, Miletto I, Caputo G, Coluccia S, Gianotti E (2008) A photoactive hybrid material based on Ru complex in mesoporous MCM-41. Nuovo Cimento B 123(10–11):1449–1458
22. Ogawa M, Nakamura T, Mori J, Kuroda K (2000) Luminescence of Tris(2,2′-bipyridine)ruthenium(II) Cations ($[Ru(bpy)_3]^{2+}$) adsorbed in mesoporous silica. J Phys Chem B 104:8554–8556
23. Fang M, Wang Y, Zhang P, Shougui L, Xu R (2000) Spectroscopic and vapochromic properties of MCM-48-entrapped trisbipyridineruthenium (II). J Lumin 91(1–2):67–70
24. Sohmiya M, Sugahara Y, Ogawa M (2007) Luminescence of Tris (2, 2′-bipyridine)ruthenium(II) Cations ([Ru(bpy)3]2+) adsorbed in mesoporous silica modified with sulphonated phenetyl group. J Phys Chem B 111(30):8836–8841
25. Suzuki K, Ikari K, Imai H (2004) Synthesis of silica nanoparticles having a well-ordered mesostructure using a double surfactant system. J Am Chem Soc 126(2):462–463
26. Slowing I, Trewyn BG, Lin VSY (2006) Effect of surface functionalization of MCM-41-type mesoporous silica nanoparticles on the endocytosis by human cancer cells. J Am Chem Soc 128 (46):14792–14793
27. Radu DR, Lai C-Y, Jeftinija K, Rowe EW, Jeftinija S, Lin VS-Y (2004) A polyamidoamine dendrimer-capped mesoporous silica

nanosphere-based gene transfection reagent. J Am Chem Soc 126:13216–13217
28. Kresge CT, Leonowicz ME, Roth WJ, Vartuli JC, Beck JS (1992) Ordered mesoporous molecular-sieves synthesized by a liquid-crystal template mechanism. Nature 359(6397):710–712
29. Du F, Liu J, Yu S, Li L (2008) Preparation and characterization of Pd/Si-MCM-41 with high hydrogenation activity. J Porous Mater 15(6):613–617
30. Li Y, Yan B (2009) Photophysical properties of lanthanide hybrids covalently bonded to functionalized MCM-41 by modified aromatic carboxylic acids. J Fluoresc 19(2):191–201
31. Krenske D, Abdo S, Van Damme H, Cruz M, Fripiat JJ (1980) Photochemical and photocatalytic properties of adsorbed organo-metallic compounds. 1. Luminescence quenching of Tris(2, 2′-bipyridine)ruthenium(II) and—chromium(III) in clay membranes. J Phys Chem 84:2447–2457